communications biology

ARTICLE

https://doi.org/10.1038/s42003-023-05487-6 OPEN

Conformational ensemble-dependent lipid recognition and segregation by prenylated intrinsically disordered regions in small GTPases

Mussie K. Araya[1] & Alemayehu A. Gorfe[1,2]✉

We studied diverse prenylated intrinsically disordered regions (PIDRs) of Ras and Rho family small GTPases using long timescale atomistic molecular dynamics simulations in an asymmetric model membrane of phosphatidylcholine (PC) and phosphatidylserine (PS) lipids. Here we show that conformational plasticity is a key determinant of lipid sorting by polybasic PIDRs and provide evidence for lipid sorting based on both headgroup and acyl chain structures. We further show that conformational ensemble-based lipid recognition is generalizable to all polybasic PIDRs, and that the sequence outside the polybasic domain (PBD) modulates the conformational plasticity, bilayer adsorption, and interactions of PIDRs with membrane lipids. Specifically, we find that palmitoylation, the ratio of basic to acidic residues, and the hydrophobic content of the sequence outside the PBD significantly impact the diversity of conformational substates and hence the extent of conformation-dependent lipid interactions. We thus propose that the PBD is required but not sufficient for the full realization of lipid sorting by prenylated PBD-containing membrane anchors, and that the membrane anchor is not only responsible for high affinity membrane binding but also directs the protein to the right target membrane where it participates in lipid sorting.

[1] McGovern Medical School, University of Texas Health Science Center at Houston, Department of Integrative Biology and Pharmacology, 6431 Fannin St., Houston, TX 77030, USA. [2] Biochemistry and Cell Biology Program & Therapeutics and Pharmacology Program, UTHealth MD Anderson Cancer Center Graduate School of Biomedical Sciences, Houston6431 Fannin St.TX 77030, USA. ✉email: Alemayehu.G.Abebe@uth.tmc.edu

Cells use primarily two types of signals to target proteins to membrane surfaces: modular protein domains and lipid-based motifs[1]. Modular membrane-targeting protein motifs such as C1, C2, PH, and BAR domains have been studied extensively (ref. [1,2] and references therein). Another class of well-studied membrane-targeting motifs utilizes a combination of an amphipathic helix and a cluster of basic residues for lipid binding (e.g.,[3,4]). Many proteins also use intrinsically disordered regions (IDRs) for membrane binding, and rules are emerging regarding their lipid recognition propensities such as preferences of basic amino acids for anion membranes[5]. While most lipid-based membrane-targeting motifs also harbor IDRs[2,6,7], insights derived from non-lipidated and autonomously membrane interacting IDRs are not directly applicable to cases where co- or post-translational lipid modification is an absolute requirement for membrane binding. This is the case, for example, in the Ras superfamily of prenylated small GTPases. As a result, our understanding of lipid recognition by lipidated IDRs remains limited despite useful insights from molecular dynamics (MD) simulation studies of Ras proteins[8]. An important open question of particular interest is how a lipidated IDR might engage and sort distinct membrane lipid species.

Membrane binding of Ras superfamily proteins requires post-translational prenyl (farnesyl or geranylgeranyl) lipid modification at a C-terminal cysteine residue[9], a tightly regulated process that also controls the cellular localization and activity of Ras and other signaling proteins[10,11]. High affinity membrane binding is often achieved by complementing the prenyl modification by a proximal polybasic domain (PBD) or an additional lipid modification[12–14]. The PBD is located within a ~10–20 residue-long flexible region, which we refer to as the prenylated intrinsically disordered region (PIDR). It is comprised of 4–8 contiguous or semicontiguous (i.e., separated by no more than two amino acids) lysine and/or arginine residues. Typical examples of PBD-containing PIDRs in the Ras superfamily include the plasma membrane (PM) associated KRAS4B (hereafter KRAS) and RhoA whose mutation or over-expression is known to cause cancers. These proteins achieve high affinity membrane binding through a combination of van der Waals (vdW) interactions of the prenyl chain with membrane lipid acyl chains and electrostatic interactions of the PBD with the headgroup of anionic lipids, such as phosphatidylserine (PS), in the inner leaflet of the PM[11–13,15]. The membrane anchor also plays a crucial role in the spatial distribution of RAS proteins on the PM[9,16–18]. Intriguingly, the specific sequence position of the basic residues in the PBD and the identity of the prenyl group were found to be important determinants of membrane binding and lipid sorting by KRAS[19–23] and Rac1[24]. Moreover, we recently showed that the interactions of the KRAS PBD with PS lipids varies with its backbone conformational dynamics (i.e., we observed ensemble-based lipid recognition)[23,25], and that charge-preserving mutations within the PBD caused changes in lipid recognition[25]. We therefore proposed that the conformational plasticity of the PIDR allows for the PDB and the prenyl group to act as a combinatorial code for lipid sorting by all PBD-containing prenylated small GTPase[25]. A primary goal of the current work is to formally test this hypothesis.

PBD-containing PIDRs differ in sequence length and net positive charge as well as in the ratio of Lys to Arg residues within the PBD. Differences within the region N-terminus to the PBD include the presence or absence of additional lipid modifications, hydrophobic content, and the ratio of basic to anionic amino acids. Another factor to consider is the spacing of the PBD from the prenylation site. If lipid sorting is sensitive to structural fluctuations of the PIDR as found in KRAS[23], how would these differences affect the membrane localization and lipid interaction of PBD-containing PIDRs? A second goal of this study is to examine the impact of these variations on PIDR structure, dynamics, and membrane binding. To this end, we studied five diverse PM targeting, PBD-containing PIDRs in a compositionally asymmetric PC/PS bilayer. These include the 19-residue-long PIDRs of Rap1A and Rap1B from the Ras family and Rac1 and Cdc42b from the Rho family. These PIDRs differ in sequence within the PBD and in the spacing of the PBD from the prenylation site, as well as in additional lipidation, hydrophobic residue content, and ratio of basic to acidic residues outside the PBD. We have also examined shorter PIDRs, one from RhoA with a similar PBD to those of the other PIDRs and another from Rheb that does not have a PBD.

These systems were investigated using atomically detailed MD simulations of 58μs aggregate effective time. The results confirm the key role of backbone conformational plasticity in lipid recognition, and further show that the sequence outside the PBD plays an important role in the adsorption of the entire peptide onto the host anionic monolayer, lipid sorting, and interaction patterns. Moreover, while the spacing of the PBD from the prenyl group has a negligible effect, palmitoylation as well as the ratio of basic to acidic residues and the hydrophobic content of the sequence N-terminal to the PBD significantly impact the diversity of conformational substates and hence the extent of conformation-dependent PS interactions.

Results

We used long timescale atomistic MD simulations (aggregate effective time = 58 μs) to investigate the membrane binding behavior, structure, and dynamics of prenylated intrinsically disordered regions (PIDRs) representing a diverse set of polybasic membrane-targeting motifs of small GTPases (Table 1 and Fig. 1; see also Supplementary Table 1 for abbreviations). These included

Table 1 The membrane-targeting prenylated intrinsically disordered regions (PIDRs) of small GTPases investigated in this work.

PIDR	Sequence length (SL)	Lipid modification		PBD		N-term to PBD		C-term to PBD	# of atoms	Sim. Length (μs x pept*)
		Prenyl	Palm	Np	K:R	Nh	B:A	S		
Rheb	12	Farn	-	-	-	-	-	-	66459	3 × 3
RhoA	10	GG	-	5	3:2	-	-	2	63708	3 × 3
Rap1A	19	GG	-	6	6:0	0.30	3:1	1	61000	10 × 3
Rap1B	19	GG	-	4	3:1	0.45	3:0	2	64063	10 × 3
Rac1	19	GG	yes	6	4:2	0.83	1:1	0	72887	10 × 1
Cdc42b	19	GG	-	4	2:2	0.70	0:4	0	63079	10 × 3

Farn farnesyl, *GG* geranylgeranyl, *Palm* palmitoyl, *PBD* polybasic domain, *Np* number of basic residues, *K:R* ratio of Lys to Arg residues, *Nh* the fraction of hydrophobic residues, *B:A* ratio of basic to acidic residues, *S* spacing between the last PBD residue and the prenylated Cys. See Table S1 for a detailed definition of these abbreviations. *The shorter Rheb and RhoA were simulated for 3μs and the rest for 10μs each, with 3 peptides per system (in Rac1 only one peptide was analyzed since the Palm in the other two did not fully insert into the bilayer). The partially pre-inserted (during setup) prenyl chains have completely and quickly inserted deep into the bilayer.

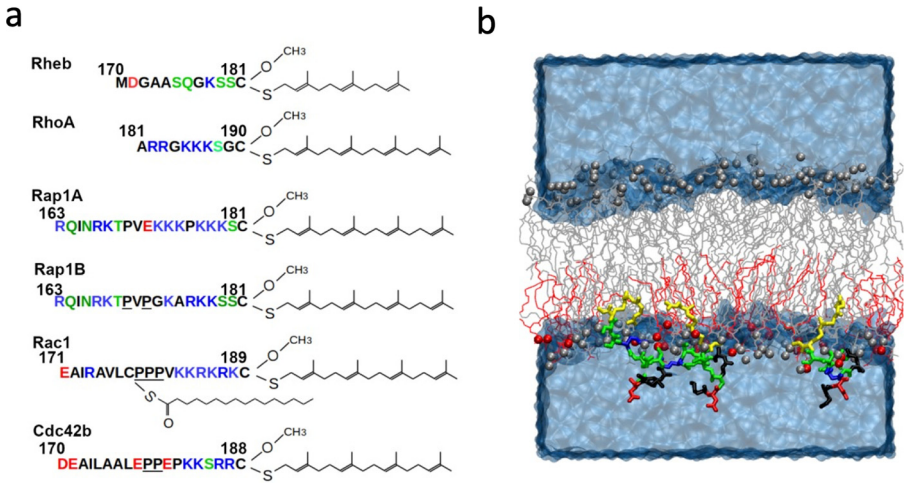

Fig. 1 Prenylated intrinsically disordered regions of small GTPases investigated in this work and simulation setup. a The amino acid sequence and lipid-modification of the simulated PIDRs (color code: basic blue; acidic red; polar green; hydrophobic black). The C-terminal Cys residue is carboxymethylated following farnesylation (Rheb) or geranylgeranylation (all others). Rac1 is also palmitoylated at residue 178. 2–3 sequentially proximal prolines are underlined. **b** An example of the simulation setup, with three peptides embedded in the mixed-lipid leaflet of an asymmetric model membrane composed of POPC (gray) and POPS lipids (red). Lipid phosphorus atoms are shown in vdW spheres and the peptides (in this case Rheb) in licorice colored as in **a**, except for the prenylated Cys residues which are in yellow. Water and ions are shown as a continuous blue surface.

Rheb, Rap1A and Rap1B from the Ras family and RhoA, Rac1 and Cdc42b from the Rho family. Each PIDR was simulated in an asymmetric PC-PC/PS bilayer to mimic the PM inner leaflet that is enriched with PS lipids.

Convergence of the simulations. As in previous observations on a PC-PC/PS bilayer of the same lipid composition[6], each of the current simulations equilibrated relatively quickly (within ~0.5–2μs). This is exemplified in Fig. 2a by the time evolutions of area per lipid (APL) and bilayer thickness (P-P) in the Rheb simulation. Supplementary Fig. 1 shows a similar trend in all systems. Bilayer stabilization was fast in Rheb and RhoA and somewhat slow in Rap1A and Rac1 (Supplementary Fig. 1). This shows that the size and complexity of the PIDR affects the speed of bilayer equilibration. We therefore simulated the shorter and fast adsorbing Rheb and RhoA PIDRs for 3 μs and the longer and hence harder to equilibrate Rap1A, Rap1B, Rac1 and Cdc42b for 10 μs each (Table 1). As noted in Methods, each simulation was started with the prenyl chain partially inserted into the bilayer. The plots of the prenyl chain insertion depth (I) versus simulation time (Fig. 2c and Supplementary Fig. 2) show that this setup allowed for a fast and complete insertion of the prenylated and oxo-methylated C-terminus, consistent with previous observations[6,26–30]. Similarly, the time evolution of backbone RMSD (Fig. 2c and Supplementary Fig. 2) shows equilibration of the simulations and convergence of the peptide structures. Together with the snapshots in Fig. 3, these results demonstrate that bilayer adsorption and structural reorganization occurred within 0.5–1 μs in all except the palmitoylated Rac1, which took longer (2.2 μs). We, therefore, excluded the first 0.5 μs (Rheb and RhoA),1 μs (Rap1A, Rap1B and Cdc42b) and 2.2 μs (Rac1) of the data from analyses of equilibrium properties. The results of these analyses are discussed in the subsequent sections.

Bilayer adsorption and membrane structure perturbation. We recently showed that PS asymmetry has only minor effects on the global structure and dynamics of a PC/PS bilayer[6]. Similar results were obtained in this work, including a slight increase in lipid packing and decrease in the lateral diffusion of lipids at the PS-containing monolayer. Since the previous analysis was based on the same lipid composition as in the current simulations, here we focus on the impact of each PIDR on bilayer structure rather than on the consequence of PS asymmetry.

The equilibrium distributions of APL and P-P displayed in Fig. 2b show that there are small differences in the ensemble-averaged bilayer thickness and area per lipid among Rheb, RhoA, Rap1A, Rap1B, and Cdc42 simulations. Compared with the farnesylated Rheb, the geranylgeranylatd RhoA caused a slight increase in bilayer thickness and a corresponding decrease in APL (Fig. 2b). This is despite the comparable sequence length of the two PIDRs and is correlated with the deeper bilayer penetration of the longer GG tail in RhoA (Fig. 2d). The two peptides also differ in bilayer adsorption, with the entire backbone of RhoA adsorbed into the headgroup region of the bilayer while part of Rheb remains in water (Fig. 3). The P-P and APL distributions in the Cdc42 simulation are very similar to those of RhoA (Fig. 2b) despite major differences in the length and sequence of the two PIDRs (Table 1 and Fig. 1). The homologous Rap1A and Rap1B have a very similar effect on P-P or APL and only slightly differ from RhoA and Cdc42b. Moreover, there are negligible differences among the GG lipidated PIDRs in insertion depth of the prenyl chain (Fig. 2d), despite notable differences in backbone adsorption (Fig. 3). Specifically, the backbone of RhoA, Rap1A and Rap1B are fully adsorbed whereas all but the last few residues of Cdc42b stayed away from the bilayer (Fig. 3). The dually lipidated Rac1 is unique in terms of both bilayer adsorption (Fig. 3) and effect on bilayer structure, characterized by a smaller average P-P and larger APL (Fig. 2b). This is due to the deep bilayer insertion of the palmitoyl chain and other hydrophobic residues in the middle of the peptide (Fig. 3). Together, these results show that the bilayer structure is perturbed more by the deep penetration of the prenyl chain and, in the case of Rac1 also the palmitoyl chain, into the hydrophobic core of the bilayer. Adsorption of the PIDR backbone in the headgroup region of the host monolayer has a smaller effect on the bilayer structure.

Structure and dynamics of PIDRs on PC-PC/PS bilayer. Supplementary Fig. 2 shows the overall convergence of the peptides in each system into a similar final structure. Minor divergences in some systems (e.g., RhoA and Rap1A) are not unexpected given the inherent structural diversity of PIDRs. We therefore

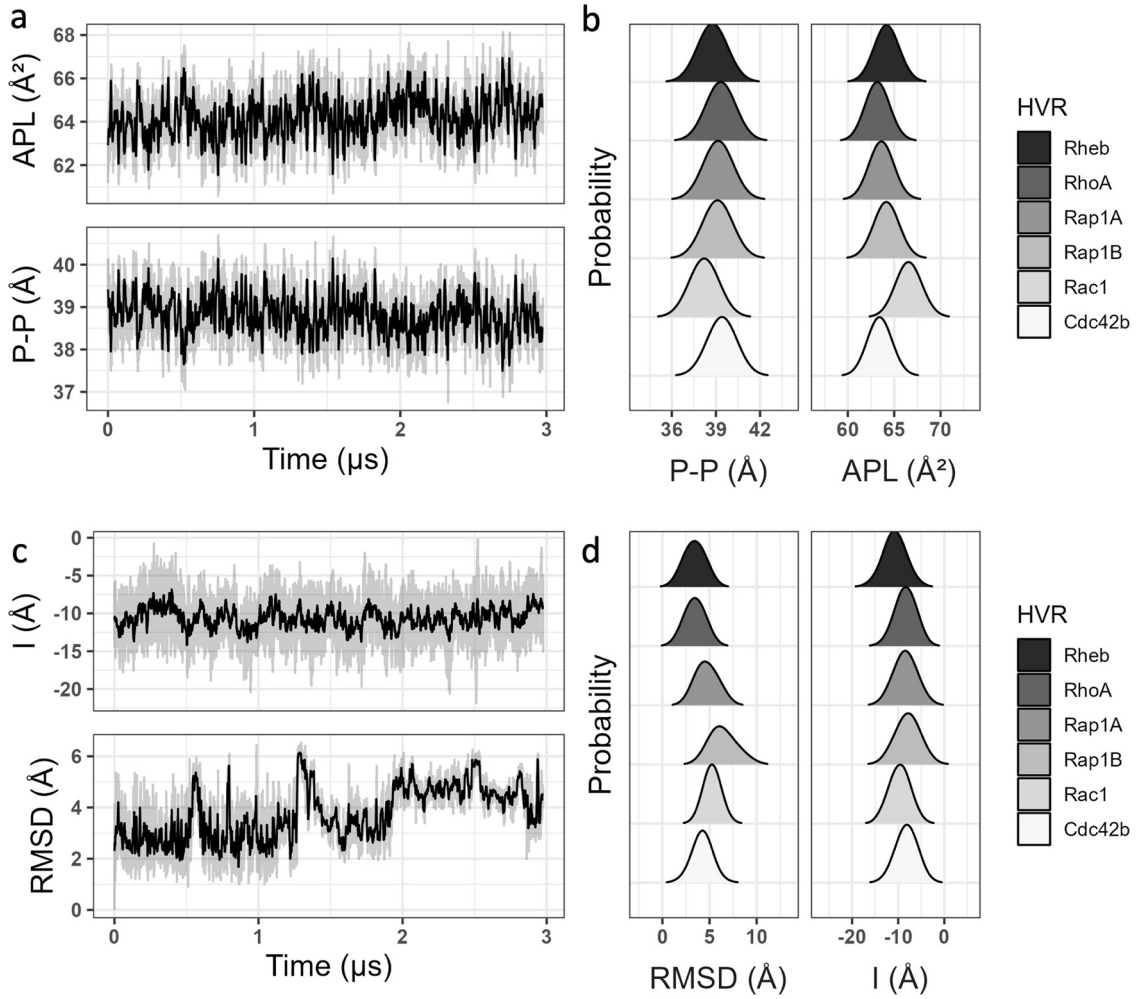

Fig. 2 Membrane and PIDR structural properties. a, **c** Time evolution of area per lipid (APL) and bilayer thickness (P-P) in the Rheb simulation (**a**), and bilayer insertion depth of the prenyl chain (I) as well as backbone root mean square deviation (RMSD) for one of the Rheb peptides (**c**). Complete sets of plots for all systems are found in Supplementary Figs. 1 and 2. **b**, **d** Histogram of P-P and APL (**b**), and RMSD and I (**d**), from each of the six simulations. In these histograms and in all subsequent figures, data from the first 0.5 μs (Rheb and RhoA), 1 μs (Rap1A, Rap1B, and Cdc42b), and 2.2 μs (Rac1) is excluded as an equilibration phase. For the PIDRs, averaging was done overall for all three peptides except for Rac1 where only one peptide was considered (see text for details). The source data behind the figure can be found in Supplementary Data 1.

considered all three peptides in all simulations for subsequent analysis except Rac1, where only one peptide that fully inserted into the bilayer was considered.

Consistent with their diversity in sequence (Fig. 1a) and bilayer adsorption profile (Fig. 3), there are significant differences among the PIDRs in the peak position and width of the time-averaged *I* and RMSD distributions (Fig. 2d). The broadness of the RMSD distributions also highlight significant structural diversity within each PIDR, which remained unstructured and highly dynamic during the simulations (Supplementary Fig. 3). For example, short helices (mostly 3_{10}) were sampled only in 3% of the frames in Rap1B, 9% in Rap1A, and <2% in all others (Supplementary Fig. 3A). Even the PEPFOD-predicted residual helicity in some PIDRs (e.g., Rap1B and Cdc42) quickly melted during the simulations (Fig. 3). Similarly, extended structures were observed only 4% of the time and only in Cdc42 (Supplementary Fig. 3a). The remaining simulated conformers are random coil (58–83%) or turn (11–40%) (Supplementary Fig. 3A). We conclude that, within the simulation timeframe, bilayer adsorption did not lead to secondary structure formation in the PIDRs studied in this work, unlike in other IDRs where such a transition has been observed[7,31–34]. However, membrane binding decreased the conformational space sampled by most PIDRs, resulting in a few well-defined conformational ensembles that are discussed later.

PIDR-bilayer localization is sequence dependent. The snapshots in Fig. 3 and the location and fluctuation of individual sidechains relative to the average location of the phosphate groups in the bilayer (Fig. 4) show that bilayer adsorption depends on the overall sequence composition of the PIDRs. As expected, the prenyl chain in each PIDR as well as the Palm tail in Rac1 inserted deep into the hydrophobic core, with their COM located about 10 Å from the average location of the phosphate group in the peptide-bound monolayer. About five residues of each PIDR immediately upstream of the prenylated Cys reside close to the phosphate group, irrespective of sequence composition and spacing of the PBD from the site of prenylation (i.e., S). This is because all five of these residues are either basic or polar that can interact with lipids through hydrogen bonding or salt bridge formation, consistent with their localization (Fig. 4). Moreover, in all cases where *S* is not zero, the intervening amino acid is Ser (Rap1A), Ser and Gly (RhoA), or two Ser residues (Rheb and Rap1B). The sidechain of Ser can form a hydrogen

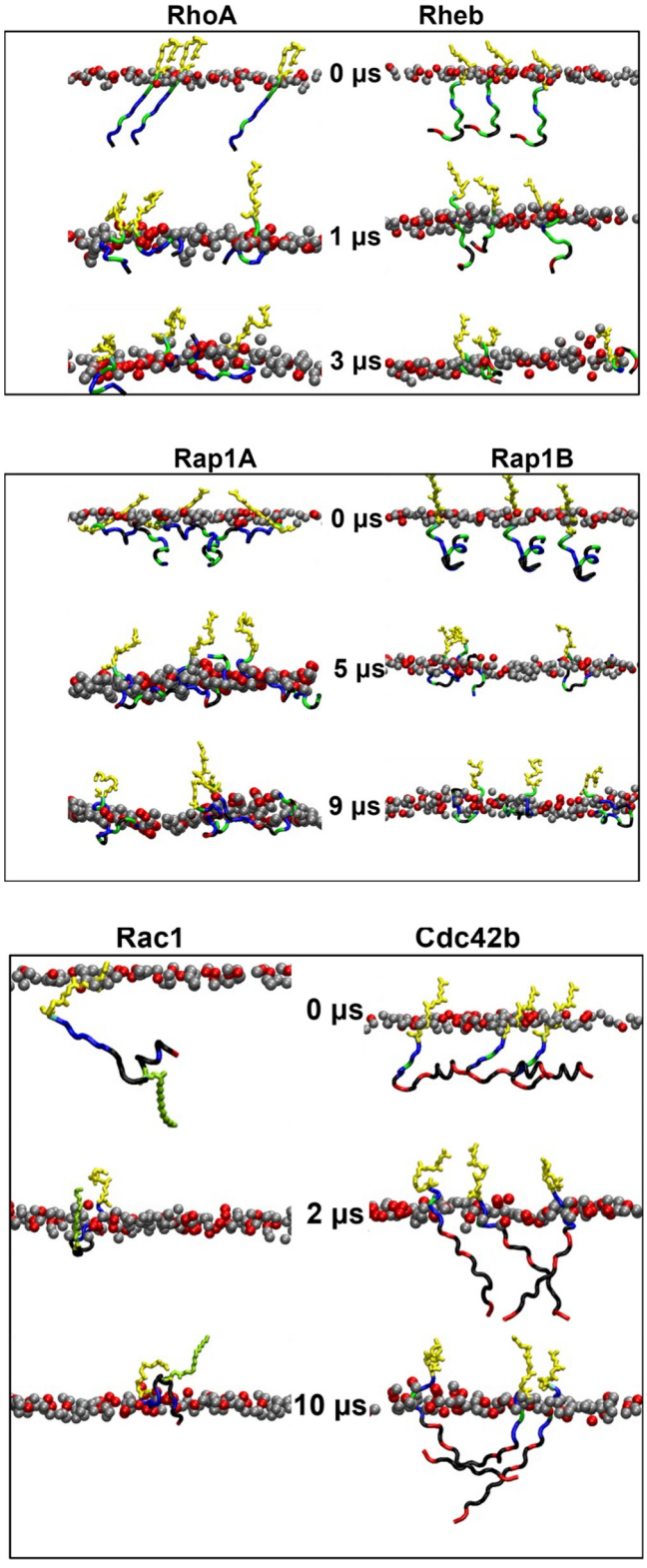

Fig. 3 Bilayer adsorption. Shown are snapshots of the membrane-embedded PIDRs at the indicated time points from each trajectory, with phosphorus atoms of POPS in red and POPC in gray (only the peptide-hosting monolayer is shown). Prenyl chain in yellow and palmitoyl in green.

with lipids and so can the Gly backbone, explaining their localization in the polar headgroup region. We conclude that *S* does not have a significant impact on the bilayer localization of the PIDRs studied in this work.

Significant differences are observed in the location of the rest of the sidechains and hence the overall organization of the PIDRs on the bilayer surface (Figs. 3 and 4). In the control peptide Rheb that does not have a PBD, almost all the sidechains apart from those near the prenylation site make only occasional contacts with lipids (see fluctuations in Fig. 4). The lack of stable interactions is also reflected in the rather diffuse distribution of the orientation of the backbone relative to the membrane normal (Supplementary Fig. 4). Similarly, the PBD-containing Cdc42b engages lipids only through the C-terminal five residues, with all other sidechains staying in water (Fig. 4) and the backbone lacking a specific orientation (Supplementary Fig. 4). This is not because Cdc42 has fewer basic residues at the PBD (Np = 4) since Rap1B with the same Np adopts a completely different bilayer-organization and orientation (Fig. 4; Supplementary Fig. 4) but rather because of the four negatively charged residues outside the PBD region (Table 1; Fig. 1a). Rap1B as well as RhoA, Rap1A, and Rac1 lie nearly flat on the bilayer surface, with the sidechains at the PBD and most of those outside the PBD residing near the lipid phosphate group (Fig. 4). RhoA, Rap1A and to a lesser extent Rap1B engage lipids through both C- and N-terminal residues, reflecting the presence of basic amino acids in these regions. These proteins also have orientational preferences (Supplementary Fig. 4). The outward bulge in the sidechain COM plot of Rap1A is caused by the single Glu in the middle of the sequence, which appears to have countered the potential impact of the neighboring non-polar sidechains (Fig. 1). By contrast, Rac1's bilayer localization is characterized by a deep insertion of the Palm tail and the neighboring hydrophobic residues, with its N-terminal Glu and other sidechains staying in water. Unlike Rap1A and Rac1 that share the same Np = 6 but differ in Nh (0.83 vs. 0.33) and B:A (3:1 vs. 1:1), Rap1B has an intermediate Nh = 0.45 and no acidic residue (B:A = 3:0). As a result, all Rap1B sidechains lie close to phosphate groups (Fig. 4) and, as in RhoA, the backbone is nearly parallel to the membrane surface (Supplementary Fig. 4). These results show that, in addition to the PBD, the sequence composition in the rest of the PIDR play key roles in membrane engagement.

PBD-containing PIDRs segregate lipids in a sequence dependent manner. What is the reason for, or the consequence of, the differential bilayer-organization of the PIDRs? To answer this question, we examined the overall interaction of each PIDR with PC and PS lipids. To do this, we counted the number of hydrogen bonds (N_{HB}) between all polar or charged amino acids and all lipid headgroup oxygen atoms, and vdW contacts (N_C) between all carbon atoms of non-polar residues (including prenyl and Palm chains but not proline) and acyl chains of lipids. In each case, averages were taken over three peptides ($N_{peptide} = 3$) in the simulation box except for Rac1 where $N_{peptide} = 1$. The time series of N_{HB} and N_C show that interactions with PS headgroup and acyl chains increased very quickly (typically within 0.1–1μs) in all the PBD-containing PIDRs (Supplementary Fig. 5). Interactions with PC remained unchanged or decreased over time except for Rac1 where there was an increase in N_C up to ~2μs, reflecting the slow insertion of the Palm chain discussed above. Remarkably, the increase in interactions with POPS headgroups (N_{HB}(PS)) is quickly followed by a corresponding increase in interactions with PS acyl chain carbons (N_C (PS)). This is true for all PIDRs including RhoA that does not have hydrophobic residues, but not for Rheb that lacks a PBD. This result demonstrates the key role of the PBD in segregating and clustering anionic lipids, thus generalizing previous observations on KRAS[6,23,25,26].

As expected, N_C is dominated by the contribution from the lipidated cysteines and therefore its value is affected by the type of

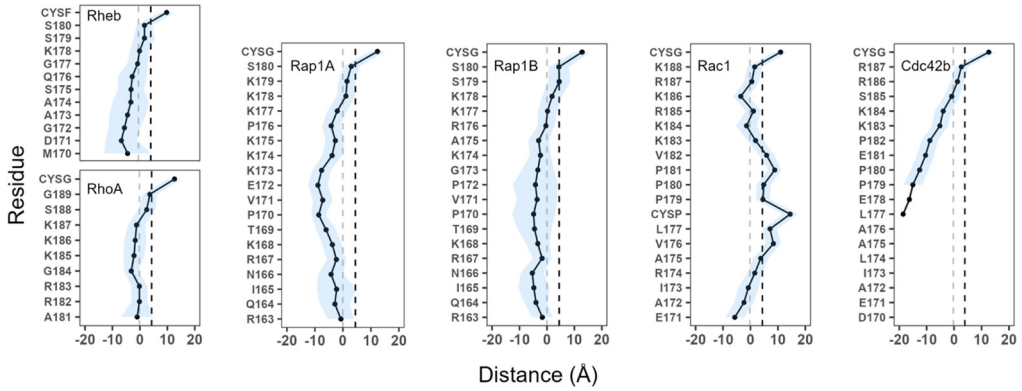

Fig. 4 Sidechain localization. Time-averaged sidechain center-of-mass z-position (mean symbols, S.D. shades) relative to the average z-position of phosphorus atoms of the host monolayer (i.e., z-distance between sidechain COM and phosphorous atoms in the host monolayer). Vertical dashed-lines indicate the average location of the POPS phosphate (gray) and glycerol-ester oxygen atoms (black). CYSF farnesylated cystine, CYSG geranylgeranylated cysteine (see Table S1 for the definition of abbreviations). The source data behind the figure can be found in Supplementary Data 2.

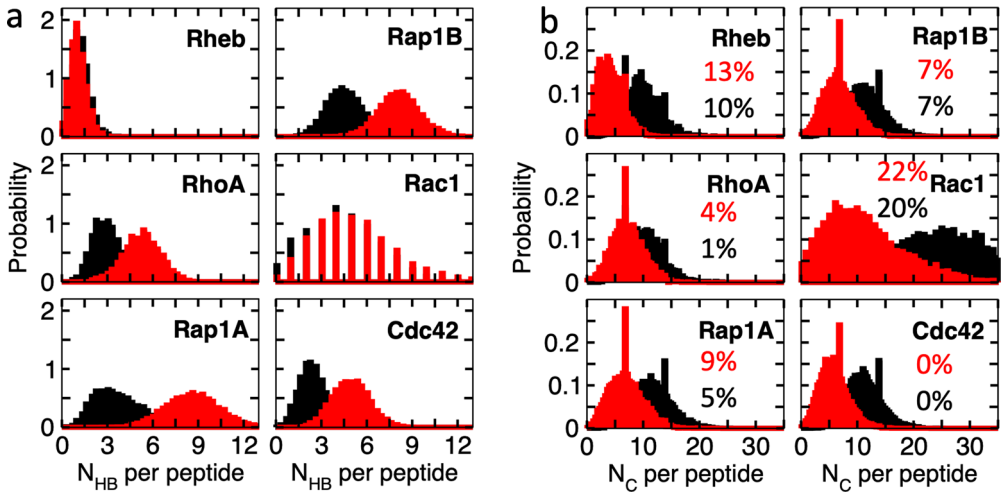

Fig. 5 PIDR-lipid interaction. Equilibrium distributions of the numbers of hydrogen bond (N_{HB}, **a**) and vdW contacts (N_C, **b**) per peptide with POPC (black) and POPS (red) lipids. HB was calculated using a donor-acceptor distance cutoff of 3.1 Å and a donor-hydrogen-acceptor angle cutoff of 30° and included all polar and charged sidechains and lipid headgroup oxygen atoms. N_C was computed using a carbon-carbon distance cutoff of 4 Å and included all non-polar sidechain carbons (excluding proline but including lipidated cysteines) and lipid acyl chain carbon atoms. The percent contributions of non-lipidated non-polar sidechains to N_C are indicated. The source data behind the figure can be found in Supplementary Data 3.

lipid modification. For example, the histograms in Fig. 5 show that the average N_C(PS) in the geranylgeranylated PIDRs varies between the narrow range of 5.8 and 7.2 but jumps to 11.2 in Rac1 because of the additional lipid modification. By contrast, N_C(PS) = 4.1 was obtained for the farnesylated Rheb. When the lipidated cysteines were excluded, we obtained N_C(PS) values of 0.3–0.6 for all except Cdc42b and Rac1 where it was 0.0 and 2.5, respectively. The latter values represent 0% and 22% of the total N_C (Fig. 5b), indicating that the non-lipidated sidechains in different PIDRs contribute differently to vdW interactions. For the longer PIDRs, these contributions are loosely correlated with Nh and B:A combined but not to either separately. Moreover, the contribution of non-lipidated amino acids to N_C is greater in the shorter Rheb than the longer Cdc42b or Rap1A, demonstrating the importance of the overall sequence composition rather than any specific variable alone. Similarly, from the histograms in Fig. 5a we find that the average N_{HB}(PS) varies between 1.3 and 8.6 and N_{HB}(PC) between 1.1 and 4.6. While it is clear that the PBD-containing PIDRs form more hydrogen bonding interactions with both PS and PC lipids, the extent of the interaction is not directly correlated with Np or K:R at the PBD but rather with the aggregate effect of both these variables and the sequence outside the PBD. For example, Rap1A (Np = 6, K:R = 6:0) and Rap1B (Np = 4; K:R = 3:1), as well as Rac1 (Np = 6; K:R = 4:2) and Cdc42b (Np = 4; K:R = 2:2), have comparable numbers of HB contacts with both PC and PS lipids despite their significant differences at the PBD (Fig. 5a). We conclude that N_H and N_C do not correlate with just Np, Nh, K:R or B:A but rather with a complex mix of these variables.

We previously showed that the KRAS PIDR preferentially engages anionic lipids primarily through salt bridge interactions between the basic residues of the PBD and the charged headgroup of lipids[23,26]. Similarly, Supplementary Fig. 6 shows a stronger interaction between Arg/Lys residues of the PIDRs studied here with the headgroup carboxyl than phosphate oxygens of POPS, except for the PBD-lacking Rheb and the deeply inserting Rac1 whose preference for phosphate and carboxyl oxygen atoms is similar. Furthermore, the equilibrium distributions of N_{HB} clearly show preference for POPS over POPC by all the PBD-containing PIDRs (Fig. 5a), and this preference resulted in preferential vdW interactions (N_C) as well. For example, for RhoA we find mean values of N_{HB}(PS) = 5.3, N_{HB}(PC) = 3.0, N_C(PS) = 7.2, and

N_C(PC) = 10.1. When we consider the PC/PS ratio of 2.3 in the host monolayer, these values indicate 4-fold and ~2-fold PS enrichment at the headgroup and acyl chain regions, respectively. Similarly, the N_{HB}(PS) and N_{HB}(PC) distributions for Rap1A and Rap1B suggest 5.4-fold and 4.1-fold PS enrichment at the headgroup, respectively. The PS enrichment at the acyl chain level estimated from the N_C(PS) and N_C(PC) distributions is ~1.5-fold in both proteins. Even in Rac1 and Cdc42b, which represent extreme cases of PBD-containing PIDRs (see next section), PS is enriched by ~2-fold and ~1.2-fold at the headgroup and acyl chain levels, respectively (Fig. 5). In the control Rheb, which has only one Lys and a few serine residues, the average N_{HB}(PS) and N_{HB}(PC) are very small and nearly equal: 1.3 and 1.1. While this suggests a 3-fold enrichment of PS at the headgroup the N_C distributions are consistent with the proportion of the PC/PS lipids, suggesting no lipid sorting at the acyl chain level. Notice in Supplementary Fig. 5 that PS lipids first engage PIDRs through HBs and then vdW contacts, and that contact with PS increases and those with PC decrease as sorting progresses. Together, these results not only demonstrate electrostatic-driven clustering and sorting of lipids at the headgroup but also show how that effect leads to a subsequent sorting of acyl chains. This finding provides the first direct evidence at the molecular level for our previous observations from EM spatial mapping and systematic lipid ablation and add back experiments[25], where we showed that KRAS preferentially interacts with PS species with one saturated and one unsaturated acyl chain but not with di-saturated or di-unsaturated PS.

Conformational sub-ensembles and lipid recognition. As described in "Methods", we analyzed the simulated conformers based on a global measure (Rg or RMSD, whichever has a multimodal distribution) and a local measure based on a pseudo dihedral angle involving four consecutive Cα atoms (Φ). For Rheb, a probability density plot of Φ versus Rg (P(Rg, Φ)) yielded at least two well separated clusters of conformers centered at P(Rg, Φ) = (9.29 ± 0.6 Å, 111 ± 14.3°) and (10.4 ± 1.3 Å, −116 ± 27.6°) (Fig. 6a). The two clusters together accounted for ~60% of the total simulated conformers (cluster 1 = 20%; cluster 2 = 40%). The smaller size of cluster 1 is not a result of limited sampling, because each cluster was visited by all three peptides in all simulations. Conformers in both clusters of Rheb are characterized by a bent backbone conformation, with those in cluster 1 bent in the middle while those in cluster 2 twisted near the N-terminus. These geometries allowed for the polar and hydrophobic residues in the middle of the peptide (residues 173–177) to submerge in the bilayer in cluster 1 but not in cluster 2 (Fig. 6b). The preponderance of more extended conformers in cluster 2 is apparent also from the distribution of sidechain locations averaged over the trajectory (Fig. 4). Interactions of the single Lys with POPS is equally weak in both clusters but the location of the Gly, Ala, Ser, and Gln residues in the bilayer is conformation-dependent (Fig. 6b). A similar analysis of RhoAshows two dominant sub-ensembles centered at P(RMSD, Φ) = (3.61 ± 0.16 Å, 45.6 ± 26.6°) and (2.44 ± 0.32 Å, −87.8 ± 16.9°) populated by extended and curled conformers, respectively (Fig. 6c). Each cluster accounted for 22% of the total conformers analyzed, with additional smaller clusters accounting for much of the remaining conformers. The two clusters share similarities in the bilayer insertion of the last four amino acids and in the overall interfacial localization of the remaining residues (Fig. 6d). However, there are significant variations in the location and hydrogen bonding potential of many residues within the PBD, including Arg182, Arg183, Lys185, Lys186, and Lys187 (Fig. 6d, e). This ensemble-dependent lipid recognition and variations in the PS interaction propensities of the PBD residues are consistent with previous observations on the KRAS PIDR[6,23,25].

The homologous Rap1A and Rap1B sampled 3–4 sub-ensembles (Fig. 7). In Rap1A, these included two compact (clusters 1 & 2) and two extended (3 & 4) sets of conformers (Fig. 7a). The conformations in clusters 1 and 2 centered at P(Rg, Φ) = (7.8 ± 0.3 Å, 122 ± 7°) and (9.6 ± 0.3 Å, 122 ± 7°) differ in bilayer localization from those in clusters 3 and 4 centered at P(Rg, Φ) = (11.5 ± 0.8 Å, 49.6 ± 7.1°) and (11.5 ± 0.8 Å, −96.1 ± 27°) (Fig. 7b). The major difference is the deeper bilayer penetration of the N-terminal five residues in clusters 3 and 4, which includes Arg163 and Arg167. As a result, these basic residues along with Lys168 formed HBs at higher frequencies in the curled structures (Fig. 7c). Within the PBD (residues 173–179), the frequency of HB contacts alternated between 'hot' and 'cold' in the curled while it is universally 'warm' (~ 50%) in the uncurled ensembles (Fig. 7c). Specifically, Lys173, lys175 and Lys178 barely interact with POPS in the curled conformers while all six lysines in the PBD partially engaged PS in the uncurled ones. There are also differences in HB frequency between clusters 3 and 4, which differ in Rg, and to a lesser extent between clusters 1 and 2 that differ in Φ, suggesting that lipid recognition is modulated by both global and local structural features. A similar conclusion could be drawn by comparing the two well populated clusters of Rap1B (the smaller third cluster is omitted for simplicity) (Fig. 7d–f). Centered at P(Rg, Φ) = (9.3 ± 0.6 Å, 111 ± 14°) and (10.4 ± 1.3 Å, −116 ± 28°), clusters 1 and 2 significantly differ in sidechain bilayer localization in the middle of the peptide (Fig. 7e) and to a lesser extent in HB frequency (Fig. 7f). Specifically, Arg167 and Arg176 formed persistent HB contacts in both clusters but Arg163, Lys174, Lys177 and Lys178's HB interactions differ between the clusters.

The results from the RhoA, Rap1A, and Rap1B trajectories described above provide strong evidence for the correlation between backbone conformational dynamics, membrane localization, and interactions of PBD residues with anionic lipids. Our findings also highlight how the sequence composition outside the PBD modulates these correlations. A more dramatic example for the latter is provided by Rac1 and Cdc42. Despite its deep membrane penetration (Figs. 3 and 4), the dually lipidated and more hydrophobic (Nh = 0.83) Rac1 sampled three distinct conformational substates (Fig. 8a). Substates 1 and 2, which account for 36% and 7% of the total conformers analyzed, are similar in compactness but differ in backbone planarity. The less compact cluster 3 (14%) shares the same dihedral angle with cluster 2. All are characterized by a deep insertion of the center of the peptide into the hydrophobic core of the bilayer and by a stable peptide-lipid engagement (smaller fluctuations in Fig. 8b). Despite these similarities, the three clusters differ in the HB frequency of several of the PBD residues (Fig. 8c): Lys184 and Lys188 interact with PS more in cluster 3 than in the rest while Arg174 and Arg187 dominate the interaction in cluster 2. It is worth noting that, in all three clusters, Arg185 interacts with POPS at a higher HB frequency than the other PBD residues (Fig. 8c). This may explain a previous observation where mutation of Arg185, but not the other PBD residues, to Gln resulted in a significant reduction in recruitment to the PM[24]. Moreover, the Rac1 PBD formed less frequent HBs than RhoA, Rap1A or Rap1B (Figs. 5a and 8c), likely because in Rac1 electrostatic interactions are complemented by a higher number of vdW contacts (Fig. 5b) involving Val176, Leu177, Palm178 and Val182 that persist in all clusters.

Cdc42b shares similarities with Rap1B at the PBD (Np = 4 in both; K:R = 2:2 vs. 3:1) but the two significantly differ in the region N-terminus of the PBD (Nh = 0.70 vs. 0.45; B:A = 0:4 vs. 3:0) (Fig. 1a). Cdc42b also shares similarity with Rac1 in terms of Nh, but the latter has a Palm chain plus two additional Lys residues at the PBD while the former has three more acidic residues outside the PBD (B:A = 0:4 vs. 1:1). However, the P(RMSD, Φ) plot of Cdc42b displayed in Fig. 8d shows a wide distribution of conformers

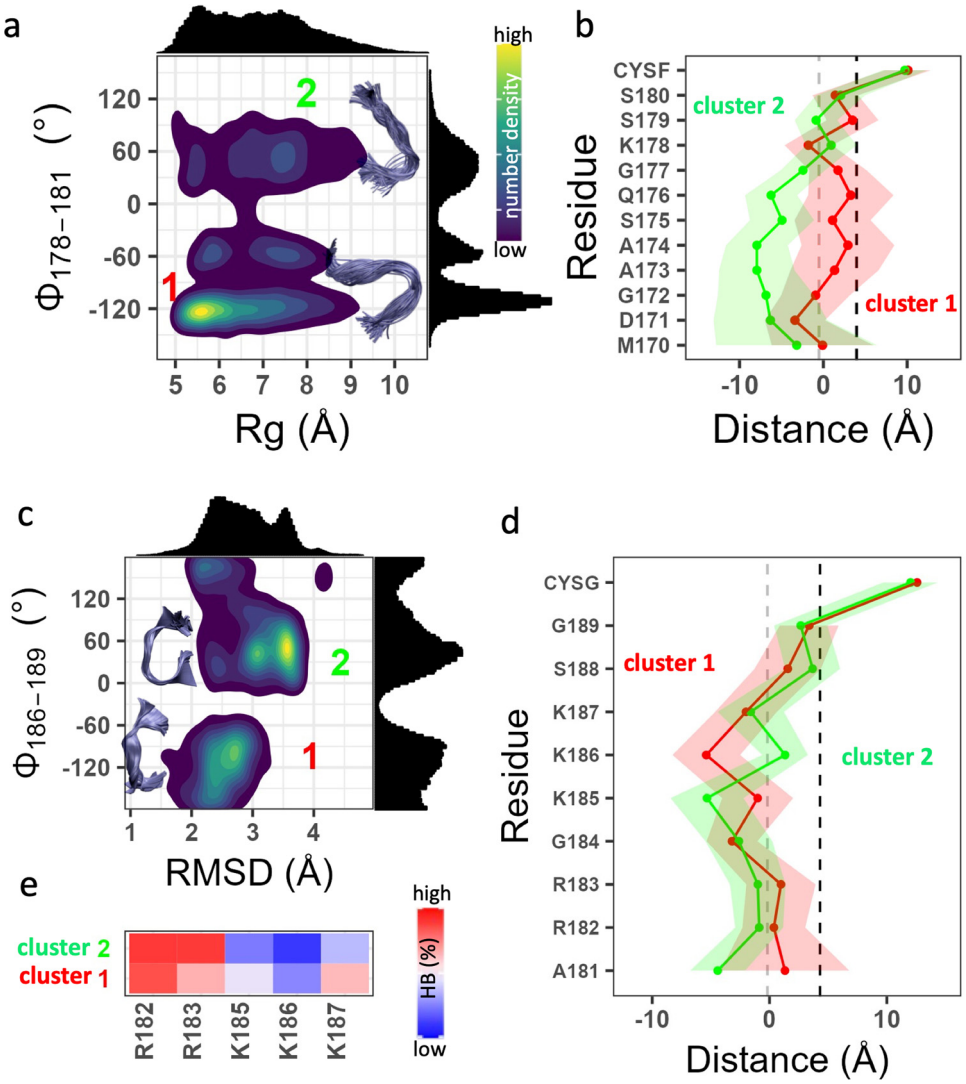

Fig. 6 Dynamics of Rheb and RhoA PIDRs on membrane. a, **c** Normalized 2D probability density distribution of Rheb (**a**) and RhoA (**c**) based on a pseudo dihedral angle defined by the Cα atoms of indicated residues (Φ) and radius of gyration (Rg) or RMSD. Histograms of Rg/RMSD and Φ are shown at the top and right of the density plot, respectively. Insets: representative backbone conformations in clusters 1 and 2 (within 1σ of the peaks). Color scale: dark blue through yellow represent 25% through 100% occupancy. **b**, **d** Time-averaged sidechain center-of-mass position of each residue in cluster 1 (red) and cluster 2 (green) of Rheb (**b**) and RhoA (**d**) relative to the average phosphate z-position of the host leaflet. **e** Heatmap of normalized hydrogen bonding frequency (HBs) between the PBD sidechains of RhoA and POPS headgroup oxygen atoms. Averaging was done over ~75,000 conformers for each system. The source data behind the figure can be found in Supplementary Data 4.

that lack the well-resolved clusters observed in the other systems. Cdc42b is also unique in its bilayer adsorption and dynamics (Figs. 3 and 4), and the absence of conformational preferences is reflected in the lack of specific orientational states (Supplementary Fig. 3). As a result of these fluctuations, only the C-terminal Arg186 and Arg187 make persistent HB contacts with POPS while Lys184 and Lys185 that often point away from the bilayer (Fig. 8e) make only sporadic HB contacts. The N-terminal region remains solvated despite carrying a hydrophobic patch (residues 172–177) that is flanked by acidic residues.

Discussion

In the current work, we used atomistic simulations to investigate six carefully selected prenylated intrinsically disordered membrane anchors of Ras and Rho family small GTPases. Ras and Rho are classical examples of molecular switches that share a conserved catalytic domain but diverge in their membrane-targeting motifs and functions. The biochemical function of these proteins involves cycling of the catalytic domain between an active GTP-bound and inactive GDP-bound states. While regulated cycling between these states is required for a wide variety of physiological processes that control cell growth, motility and trafficking[35–37], dysregulation of the cycle causes many intractable diseases including cancer[38–45]. In addition to the GTPase cycle, membrane binding is required for the cellular activity of Ras and Rh. However, our insight into the structure and dynamics of these proteins in membrane is limited. In the past, we and others have studied the membrane insertion profile[26,30,46] and energetics[47–49] of the isolated lipid anchor (as well as the HVR[30,50]) of Ras proteins using MD simulations. We have combined MD simulations with cell signaling assays, EM, or single molecule FRET studies to show that the catalytic domain of Ras proteins interacts with membrane in multiple orientations[27–29,46,51]. Some of these orientations are defective in signal transduction due to occlusion of the effector-binding region by the membrane[27,52]. We have also shown that the sequence and dynamics of the KRAS

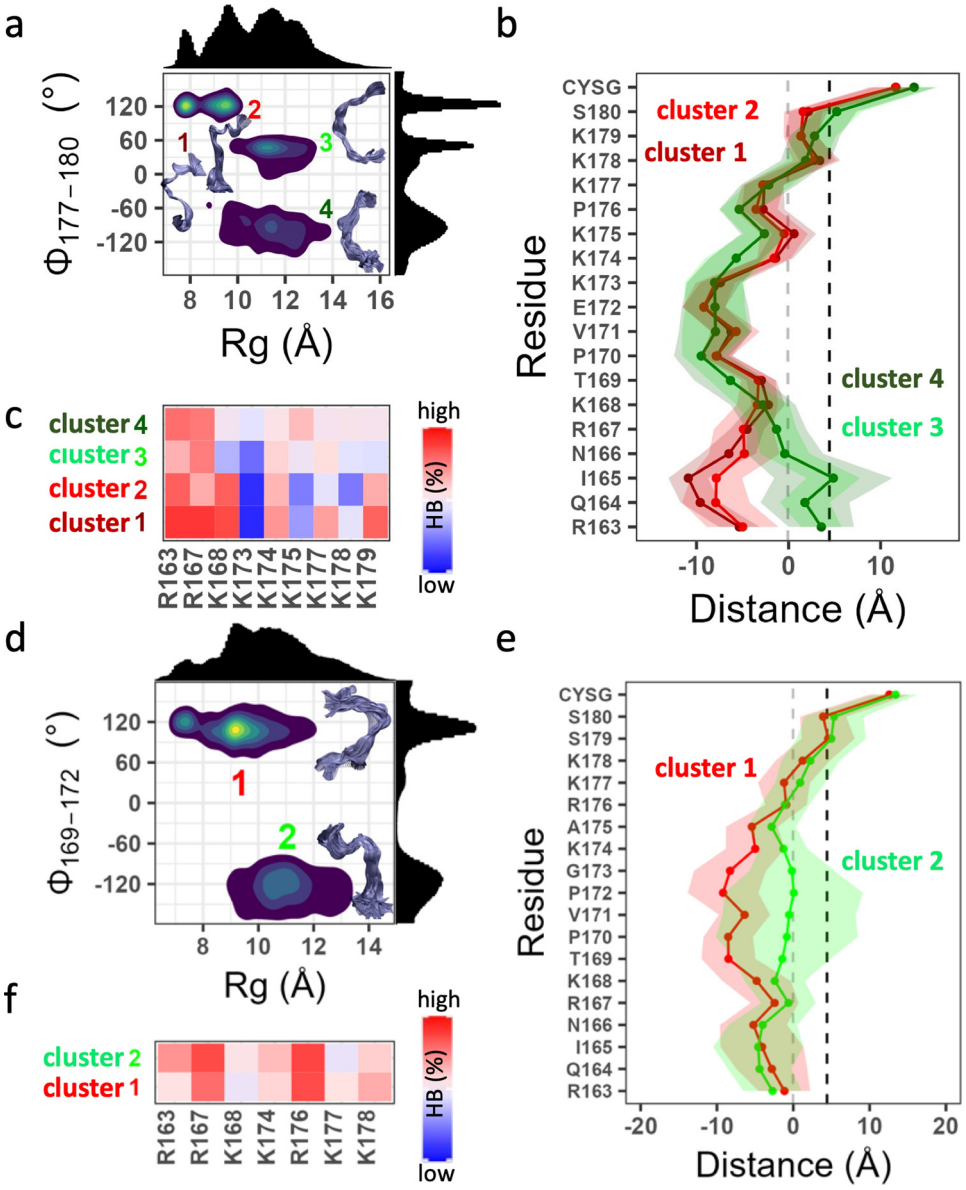

Fig. 7 Dynamics of Rap1A and Rap1B PIDRs on membrane. a–c show that the PIDR of Rap1A fluctuates between four conformational substates (**a**) that adopt two distinct bilayer adsorption profiles (**b**) and ensemble-dependent interactions with POPS (**c**). **d–f** show that the Rap1B PIDR samples at least two distinct conformational substates (**d**) that differ in bilayer adsorption (**e**) and PS interaction (**f**). Averages were taken over ~250,000 conformers for each protein. Color code is as in Fig. 6. The source data behind the figure can be found in Supplementary Data 5.

lipid anchor encode lipid selectivity[23,25] and the conformational dynamics of the HVR is a key determinant of membrane reorientation[27–29]. The current work generalizes these intriguing findings by studying the RhoA, Rap1A, Rap1B, Rac1 and Cdc42b membrane-targeting motifs, and thereby sets the stage for future investigations of the full-length proteins using MD, EM, and functional assays as we have done in the past[23,25,28,51].

Note that RhoA, Rap1A, Rap1B, Rac1 and Cdc42b possess a polybasic domain (PBD) while Rheb does not have a PBD. In previous studies of the PBD-containing KRAS PIDR in which individual PBD residues were mutated to Gln, we observed distinct conformational distributions and patterns of interaction with anionic lipids[23,25]. Variations in conformational sampling and interaction were observed even among equally charged KRAS PBD mutants, as well as between farnesylated and geranylgeranylated KRAS anchors[25]. These findings suggested that the specific sequence composition of the PBD and the identity of the prenyl chain together determine lipid recognition by altering the conformational dynamics of the membrane anchor. The current results not only validated this hypothesis but also extended it in many respects, such as by demonstrating the significance of the amino acid sequence outside the PBD (Figs. 3–8).

In RhoA, Rap1A and Rap1B, interactions of the PBD Arg and Lys residues with anionic lipids varied with the conformational ensembles of the backbone (Figs. 6 and 7). In addition, not all PDB residues engaged lipids in all ensembles, with some side-chains interacting with POPS only when the backbone adopts a particular conformation. Moreover, Arg forms stronger (more frequent) salt bridge/hydrogen bonds with PS than Lys. All these observations are consistent with our previous results[23,25,26], and demonstrate that conformation-dependent interaction with anionic lipids is generalizable to prenylated PBD membrane anchors. The current results also suggest a strong correlation of interaction patterns with bilayer adsorption profiles (Fig. 3),

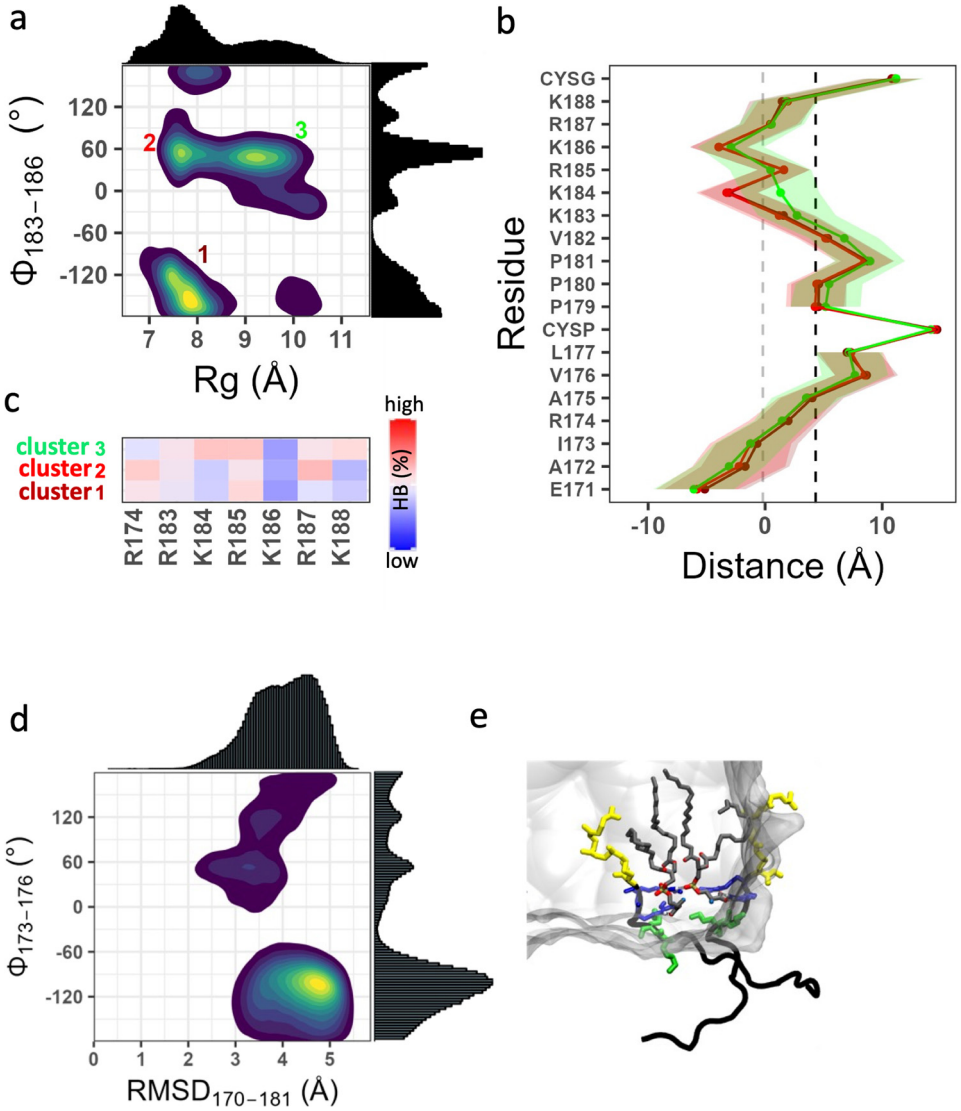

Fig. 8 Dynamics of Rac1 and Cdc42b PIDRs on membrane. a–c Three clusters are observed in Rac1 (**a**) that differ little in bilayer adsorption (**b**) but differ in interaction with POPS (**c**). **d**, **e** Cdc42 does not sample defined conformational ensembles (**d**) with only Arg186 and Arg187 (blue) interacting with POPS while Lys183 and Lys184 (green) point away from the bilayer (**e**). The prenyl group is in yellow licorice and POPS in gray licorice, with oxygen atoms in red and P atoms in gold. Averaging was over ~78,000 conformers for Rac1 and ~250,000 conformers for Cdc42. CYSP palmitoylated cysteine. The source data behind the figure can be found in Supplementary Data 6.

localization of sidechains (Fig. 4), and orientation of the PIDR relative to the bilayer surface (Supplementary Fig. 4). We propose that these correlations, too, are generalizable to classical prenylated PDB anchors where the PIDR sequence outside the PBD is enriched with basic amino acids like in Rap1A and Rap1B (Fig. 1a). Other examples of RAS family proteins with a classical prenylated PDB include RAL1A, RAL1B, MRAS, DIRAS1, DIRAS2, RASD1, RASL10A and RASL10B.

The Rac1 and Cdc42 membrane anchors represent two extremes of the sequence diversity in PBD-containing PIDRs. The Rac1 PIDR is enriched with non-polar residues and is palmitoylated in addition to being prenylated. While palmitoylated and prenylated PIDRs are common in small GTPases such as in NRAS, HRAS, KRAS4A, RAP2A, RAP2B and ERAS in the RAS family as well as RhoB in the Rho family, palmitoylated and prenylated PIDRs containing a PBD are rare (the only other example in the Rho family is RhoJ). Our Rac1 results suggest that conformation-dependent interaction with anionic lipids also occurs in these rare PIDRs, with some variations in the details (Fig. 8). We also found that unlike RhoA, Rap1A or Rap1B, membrane binding of Rac1 is dominated by vdW interactions (Figs. 5 and 8). At the other end of the spectrum is Cdc42b, which has no basic residues outside the PBD but instead has four acidic residues (B:A = 0:4). For comparison, all the prenylated PBD-containing small GTPases mentioned above have a highly conserved ~20 residues-long PIDR with a high proportion of polar plus basic (but not acidic) residues, consistent with their primary location at the anionic inner leaflet of the PM. The unique sequence composition of Cdc42b's PIDR is responsible for its inability to fully adsorb on the PS-rich anionic model membrane (Figs. 3 and 4), and for the lack of conformation-dependent HB contacts with lipids (Fig. 8). Together, the Rac1 and Cdc42b results strongly suggest that conformation-dependent lipid sorting by prenylated PBD membrane anchors is fine-tuned by the sequence composition of the flexible segment preceding the PBD. In other words, the PBD is required but may not be sufficient for a full realization of ensemble-based lipid sorting by polybasic PIDRs. This can be tested, for example, by mutating individual

residues within and outside the PBD and examining their impact on membrane binding and nanoclustering using EM spatial mapping, as we have done in the past[23,25].

Additional support for the relevance of bilayer adsorption of the entire PIDR in stabilizing a set of well-defined conformational ensembles is provided by the Rheb control simulation (Fig. 6). In the relatively few instances in which this peptide was able to fully adsorb on the bilayer, it adopted a more stable conformation characterized by a sharp peak of dihedral angle versus radius of gyration plot (cluster 1 in Fig. 6). However, this state is sampled rarely due to the lack of stabilizing electrostatic interactions. The phase space sampled by the non-adsorbed conformers is wide (cluster 2 in Fig. 6), like that of Cdc42 (Fig. 8). It is possible, however, that both Cdc42 and Rheb PIDRs will sample a more defined set of conformational ensembles when bound to a bilayer of different lipid composition, in the presence of minor lipid species such as PIP2, or, in the case of Cdc42, if the acidic residues are sequestered by a binding partner. This suggests a direct relationship between the sequence of the entire PIDR and the lipid composition of the target membrane. If confirmed by additional studies such as with mutagenesis and EM spatial mapping, a major inference of significant biological relevance that follows is that lipid recognition and sorting may be encoded in the intrinsically disordered membrane anchor of *all* lipidated peripheral membrane proteins. This means that the membrane anchor is not only responsible for high affinity membrane binding but also directs the protein to the right target membrane where it participates in lipid sorting.

The current results also provide an explanation for an intriguing previous observation where we found that KRAS selectively engages PS species with an asymmetric acyl chain saturation[25]. Our finding that electrostatic-driven sorting of PS lipids at the headgroup ultimately leads to selective interactions at the acyl chain level (Fig. 5 and Supplementary Fig. 4) provide a detailed insight into how PBD-containing membrane anchors achieve specificity for both lipid headgroup and acyl chain structures. This result has a profound implication for future studies of the cellular distribution, transport, and function of prenylated proteins with a PBD membrane anchor.

Methods

Model selection. Our goal in this work was to test the hypothesis that backbone conformational plasticity of PBD-containing PIDRs is correlated with their lipid recognition profile, and that this ensemble-based lipid recognition is tuned by the sequence length and composition of the PIDR as well as by the charge and spacing of the PBD from the prenylated cysteine. To test this hypothesis, we selected five diverse PBD-containing PIDRs as model systems, representing the membrane-targeting motifs of RhoA, Rap1A, Rap1B, Rac1 and Cdc42b (Table 1). The C-terminal Cys of all five proteins is post-translationally modified by geranylgeranylation (GG) and carboxymethylation (Fig. 1a; Supplementary Table 1). The PIDRs of Rap1A, Rap1B, Rac1 and Cdc42b have the same sequence length (SL = 19) but differ in the net charge (Np = 6, 4, 6, 4) and Lys to Arg ratio (K:R = 6:0, 3:1, 4:2, 2:2) within the PBD (Table 1 and Fig. 1a; Supplementary Table S1). They also differ in the region N-terminus to the PBD, including in terms of hydrophobic content defined as the ratio of hydrophobic to total number of residues (Nh = 0.33, 0.45, 0.83, 0.70), the ratio of basic to acidic amino acids (B:A = 3:1, 3:0, 1:1, 0:4), and the presence of a palmitoylated cysteine in Rac1. The RhoA PIDR is shorter (SL = 10) and lacks a hydrophobic N-terminal extension, but it has a comparable PBD to Rap1B (Np = 5 vs. 4; K:R = 3:2 vs. 3:1). These five proteins also differ in the spacing of the PBD from the prenylation site, *S*, defined as the number of residues between the last residue of the PBD and the prenylated cysteine. For control, we included the farnesylated (Farn) membrane-targeting motif of Rheb that has a similar SL to RhoA but lacks a PB sequence (Table 1 and Fig. 1a).

Modeling PIDR initial structures. No experimental structure is available for any of the PIDRs studied here. Therefore, we attempted to use SWISS-MODEL (https://swissmodel.expasy.org) and PEPFOLD (https://bioserv.rpbs.univ-paris-diderot.fr/services/PEP-FOLD/) servers to obtain consensus predictions of initial structures. However, only PEPFOLD yielded a complete structure for all peptides. Some of the predicted structures had a short helix but we selected models with the least amount of secondary structure with the assumption that the PIDRs are unstructured in solution. We then used CHARMM-GUI[53,54] to attach a GG or Farn lipid and oxo-methylate the C-terminal cysteine. For Rac1, a palmitoyl lipid was also added to Cys178 (Fig. 1a).

PIDR-bilayer system construction. The inner leaflet of the PM where most of the PIDRs localize is enriched both in PS and phosphatidylethanolamine (PE) lipids. However, we showed recently that when compared with a PC-PC/PS bilayer, the presence of PE in an asymmetric PC-PC/PS/PE bilayer did not significantly alter the dynamics and membrane interactions of the KRAS PIDR[6]. Therefore, here we used the simpler binary bilayer in which PS lipids are distributed only to the monolayer where peptides are bound. An initial model of such a membrane was built as described recently[6], with one leaflet containing 33 POPS and 77 POPC and the other 108 POPC lipids. This ensured area symmetry also considering the volume of the peptide lipids embedded in the mixed-lipid monolayer. To build initial PIDR-bilayer complexes, about 5 terminal carbon atoms of the prenyl chain were manually inserted into the hydrophobic core of the mixed-lipid leaflet. In this manner, we attached three peptides per system to triple sampling with the computational cost of a single peptide (peptides were spaced 30–50 Å center-of-mass distance apart to avoid self-interaction). The resulting PIDR-bilayer systems were solvated with TIP3P waters and neutralized by adding Na^+. The final systems ranged in size between 61,000 and 72,887 atoms (Table 1). An example of the final setup is shown in Fig. 1b.

Molecular dynamics simulation and trajectory analysis. Each system was energy-minimized and equilibrated as described previously[6], and then subjected to a production run of 15–23 ns using the NAMD program[55] and the CHARMM36m force field[56]. The longer PIDR systems were then simulated for 10μs and the shorter ones for 3μs each on Anton 2 (Table 1), with trajectories written out every 100 ps for analysis. Bilayer and protein structural and dynamic properties were analyzed as described in previous reports[6,26]. This included monitoring standard measures such as root mean square deviation (RMSD), radius of gyration (Rg), frequency of hydrogen bond (HB) and van der Waals (vdW) contacts, as well as bilayer thickness and area per lipid. Area per lipid (APL) was calculated from the area of the simulation box at the pure-POPC monolayer, and bilayer thickness using the average z-distance between the electron dense phosphorus (P) atoms at the two monolayers (P-P). Bilayer insertion depth, *I*, was calculated as the z-distance of the center-of-mass (COM) of the prenyl chain from the bilayer COM. HB was defined using donor-acceptor distance cutoff of 3.1 Å and angle 30°, and vdW contact using a 4.0 Å cutoff between pairs of carbon atoms. As in previous work[6,26], we used multiple reaction coordinates (RCs) to characterize the highly dynamic PIDRs. These included global measures such as Rg, RMSD, and orientation relative to the membrane normal, as well as local features such as pseudo dihedral angles (Φ) involving virtual bonds

between four consecutive Cα atoms. Φ was computed for every four consecutive residues and the one that most clearly classified the simulated conformers into sub-ensembles was used for subsequent analyses. We used R[57] and VMD[58] scripting for analysis.

Statistics and reproducibility. To ensure reproducibility and sampling of phase space, we used data from long timescale MD simulations with three copies of the peptides used in each simulation system. Where relevant, three peptide trajectories were concatenated resulting in 9 μs (Rheb and RhoA) or 30 μs (Rap1A, Rap1B and Cdc42b) effective time trajectories, except for Rac1 where only one peptide has fully inserted into the bilayer and thus the total trajectory analyzed was 10 μs. Time-averaged equilibrium structural and thermodynamic properties are reported in terms of mean and standard deviation averaged over trajectories sampled every 100 ps, excluding the first 0.5 μs (Rheb and RhoA),1 μs (Rap1A, Rap1B, and Cdc42b) and 2.2 μs (Rac1) as equilibration phase.

Reporting summary. Further information on research design is available in the Nature Portfolio Reporting Summary linked to this article.

Data availability

Initial coordinates, simulation input files, and coordinate files of final outputs in the publicly accessible repository https://github.com/mussiekar/HVRs. All other data are available from the corresponding author upon reasonable request.

Received: 15 May 2023; Accepted: 19 October 2023;
Published online: 02 November 2023

References

1. Janosi, L. & Gorfe, A. A. Interaction between proteins and biological membranes. *In:* Protein interaction: the molecular basis of interactomic. Helms and Kalinina Eds. Wiley, 293–314 (2022).
2. Araya, M. K., Zhou, Y. & Gorfe, A. A. Remodeling of the plasma membrane by surface-bound protein monomers and oligomers: the critical role of intrinsically disordered regions. *J. Membr. Biol.* **255**, 651–663 (2022).
3. Smrt, S. T., Escobar, C. A., Dey, S., Cross, T. A. & Zhou, H. X. An Arg/Ala-rich helix in the N-terminal region of M. tuberculosis FtsQ is a potential membrane anchor of the Z-ring. *Commun. Biol.* **6**, 311 (2023).
4. Dey, S. & Zhou, H. X. Membrane tethering of sepF, a membrane anchor for the mycobacterium tuberculosis Z-ring. *J. Mol. Biol.* **434**, 167817 (2022).
5. Qin, S., Hicks, A., Dey, S., Prasad, R. & Zhou, H. X. ReSMAP: web server for predicting residue-specific membrane-association propensities of intrinsically disordered proteins. *Membranes* **12**, 773 (2022).
6. Araya, M. K. & Gorfe, A. A. Phosphatidylserine and phosphatidylethanolamine asymmetry have a negligible effect on the global structure, dynamics, and interactions of the KRAS lipid anchor. *J. Phys. Chem. B* **126**, 4491–4500 (2022).
7. Cornish, J., Chamberlain, S. G., Owen, D. & Mott, H. R. Intrinsically disordered proteins and membranes: a marriage of convenience for cell signalling? *Biochem Soc. Trans.* **48**, 2669–2689 (2020).
8. Prakash, P. & Gorfe, A. A. Lessons from computer simulations of Ras proteins in solution and in membrane. *Biochim Biophys. Acta* **1830**, 5211–5218 (2013).
9. Abankwa, D. & Gorfe, A. A. Mechanisms of Ras membrane organization and signaling: Ras rocks again. *Biomolecules* **10**, 1522 (2020).
10. Wang, W. & Casey, P. J. Protein prenylation: unique fats make their mark on biology. *Nat. Rev. Mol. Cell Biol.* **17**, 110–122 (2016).
11. Jung, D. & Bachmann, H. S. Regulation of protein prenylation. *Biomed. Pharmacother.* **164**, 114915 (2023).
12. Williams, C. L. The polybasic region of Ras and Rho family small GTPases: a regulator of 658protein interactions and membrane association and a site of nuclear localization signal 659sequences. *Cell Signal.* **15**, 1071–1080 (2003).
13. Hancock, J. F., Paterson, H. & Marshall, C. J. A polybasic domain or palmitoylation is required in addition to the CAAX motif to localize p21ras to the plasma membrane. *Cell* **63**, 133–139 (1990).
14. Roy, M.-O., Leventis, R. & Silvius, J. R. Mutational and biochemical analysis of plasma membrane targeting mediated by the farnesylated, polybasic carboxy terminus of K-ras4B. *Biochemistry* **39**, 8298–8307 (2000).
15. Mulgrew-Nesbitt, A. et al. The role of electrostatics in protein–membrane interactions. *Biochim. Biophys. Acta* **1761**, 812–826 (2006).
16. Michaelson, D. et al. Differential localization of Rho GTPases in live cells: regulation by hypervariable regions and RhoGDI binding. *J. Cell Biol.* **152**, 111–126 (2001).
17. Zhou, Y. & Hancock, J. F. Ras nanoclusters: versatile lipid-based signaling platforms. *Biochim. Biophys. Acta* **1853**, 841–849 (2015).
18. Janosi, L., Li, Z., Hancock, J. F. & Gorfe, A. A. Organization, dynamics, and segregation of Ras nanoclusters in membrane domains. *Proc. Natl Acad. Sci. USA* **109**, 8097–8102 (2012).
19. Zhou, Y., Gorfe, A. A. & Hancock, J. F. RAS nanoclusters selectively sort distinct lipid headgroups and acyl chains. *Front. Mol. Biosci.* **8**, 686338 (2021).
20. Zhou, Y. & Hancock, J. F. Lipid profiles of RAS nanoclusters regulate RAS function. *Biomolecules* **11**, 1439 (2021).
21. Zhou, Y. & Hancock, J. F. A novel prenyl-polybasic domain code determines lipid-binding specificity of the K-Ras membrane anchor. *Small GTPases* **11**, 220–224 (2020).
22. Zhou, Y. & Hancock, J. F. Deciphering lipid codes: K-Ras as a paradigm. *Traffic* **19**, 157–165 (2018).
23. Zhou, Y. et al. Lipid-sorting specificity encoded in K-Ras membrane anchor regulates signal output. *Cell* **168**, 239–251.e16 (2017).
24. Maxwell, K. N., Zhou, Y. & Hancock, J. F. Rac1 nanoscale organization on the plasma membrane is driven by lipid binding specificity encoded in the membrane anchor. *Mol. Cell Biol.* **38**, e00186–18 (2018).
25. Zhou, Y., Prakash, P. S., Liang, H., Gorfe, A. A. & Hancock, J. F. The KRAS and other prenylated polybasic domain membrane anchors recognize phosphatidylserine acyl chain structure. *Proc. Natl Acad. Sci. USA* **118**, e2014605118 (2021).
26. Janosi, L. & Gorfe, A. A. Segregation of negatively charged phospholipids by the polycationic and farnesylated membrane anchor of Kras. *Biophys. J.* **99**, 3666–3674 (2010).
27. Prakash, P., Zhou, Y., Liang, H., Hancock, J. F. & Gorfe, A. A. Oncogenic K-Ras binds to an anionic membrane in two distinct orientations: a molecular dynamics analysis. *Biophys. J.* **110**, 1125–1138 (2016).
28. Prakash, P. et al. Dynamics of membrane-bound G12V-KRAS from simulations and single-molecule FRET in native nanodiscs. *Biophys. J.* **116**, 179–183 (2019).
29. Prakash, P. & Gorfe, A. A. Probing the conformational and energy landscapes of KRAS membrane orientation. *J. Phys. Chem. B* **123**, 8644–8652 (2019).
30. Gorfe, A. A., Babakhani, A. & McCammon, J. A. H-ras protein in a bilayer: interaction and structure perturbation. *J. Am. Chem. Soc.* **129**, 12280–12286 (2007).
31. Gimenez-Andres, M., Copic, A. & Antonny, B. The many faces of amphipathic helices. *Biomolecules* **8**, 45 (2018).
32. Hristova, K. et al. An amphipathic α-helix at a membrane interface: a structural study using a novel X-ray diffraction method. *J. Mol. Biol.* **290**, 99–117 (1999).
33. Fusco, G., Sanz-Hernandez, M. & De Simone, A. Order and disorder in the physiological membrane binding of alpha-synuclein. *Curr. Opin. Struct. Biol.* **48**, 49–57 (2018).
34. Jiang, X. et al. Membrane-mediated disorder-to-order transition of SNAP25 flexible linker facilitates its interaction with syntaxin-1 and SNARE-complex assembly. *FASEB J.* **33**, 7985–7994 (2019).
35. Macara, I. G., Lounsbury, K. M., Richards, S. A., McKiernan, C. & Bar-Sagi, D. The Ras superfamily of GTPases. *FASEB J.* **10**, 625–630 (1996).
36. Wennerberg, K., Rossman, K. L. & Der, C. J. The Ras superfamily at a glance. *J. Cell Sci.* **118**, 843–846 (2005).
37. Goitre, L., Trapani, E., Trabalzini, L. & Retta, S. F. The Ras superfamily of small GTPases: the unlocked secrets. *Methods Mol. Biol.* **1120**, 1–18 (2014).
38. Fritz, G., Just, I. & Kaina, B. Rho GTPases are over-expressed in human tumors. *Int J. Cancer* **81**, 682–687 (1999).
39. Schubbert, S., Shannon, K. & Bollag, G. Hyperactive Ras in developmental disorders and cancer. *Nat. Rev. Cancer* **7**, 295–308 (2007).
40. Vega, F. M. & Ridley, A. J. Rho GTPases in cancer cell biology. *FEBS Lett.* **582**, 2093–2101 (2008).
41. Vasiliev, J. M., Omelchenko, T., Gelfand, I. M., Feder, H. H. & Bonder, E. M. Rho overexpression leads to mitosis-associated detachment of cells from epithelial sheets: a link to the mechanism of cancer dissemination. *Proc. Natl Acad. Sci. USA* **101**, 12526–12530 (2004).
42. Cox, A. D. & Der, C. J. Ras history: the saga continues. *Small GTPases* **1**, 2–27 (2010).
43. Seixas, E., Barros, M., Seabra, M. C. & Barral, D. C. Rab and Arf proteins in genetic diseases. *Traffic* **14**, 871–885 (2013).
44. Bos, J. L. Ras oncogenes in human cancer: a review. *Cancer Res.* **49**, 4682–4689 (1989).

45. Karnoub, A. E. & Weinberg, R. A. Ras oncogenes: split personalities. *Nat. Rev. Mol. Cell Biol.* **9**, 517–531 (2008).
46. Gorfe, A. A., Hanzal-Bayer, M., Abankwa, D., Hancock, J. F. & McCammon, J. A. Structure and dynamics of the full-length lipid-modified H-Ras protein in a 1,2-dimyristoylglycero-3-phosphocholine bilayer. *J. Med. Chem.* **50**, 674–684 (2007).
47. Gorfe, A. A. & McCammon, J. A. Similar membrane affinity of mono- and Di-S-acylated ras membrane anchors: a new twist in the role of protein lipidation. *J. Am. Chem. Soc.* **130**, 12624–12625 (2008).
48. Gorfe, A. A., Baron, R. & McCammon, J. A. Water-membrane partition thermodynamics of an amphiphilic lipopeptide: an enthalpy-driven hydrophobic effect. *Biophys. J.* **95**, 3269–3277 (2008).
49. Gorfe, A. A., Babakhani, A. & McCammon, J. A. Free energy profile of H-ras membrane anchor upon membrane insertion. *Angew. Chem. Int. Ed. Engl.* **46**, 8234–8237 (2007).
50. Neale, C. & Garcia, A. E. Methionine 170 is an environmentally sensitive membrane anchor in the disordered HVR of K-Ras4B. *J. Phys. Chem. B* **122**, 10086–10096 (2018).
51. Abankwa, D., Gorfe, A. A., Inder, K. & Hancock, J. F. Ras membrane orientation and nanodomain localization generate isoform diversity. *Proc. Natl Acad. Sci. USA* **107**, 1130–1135 (2010).
52. Mazhab-Jafari, M. T. et al. Oncogenic and RASopathy-associated K-RAS mutations relieve membrane-dependent occlusion of the effector-binding site. *Proc. Natl Acad. Sci. USA* **112**, 6625–6630 (2015).
53. Lee, J. et al. CHARMM-GUI membrane builder for complex biological membrane simulations with glycolipids and lipoglycans. *J. Chem. Theory Comput* **15**, 775–786 (2019).
54. Jo, S. et al. CHARMM-GUI 10 years for biomolecular modeling and simulation. *J. Comput Chem.* **38**, 1114–1124 (2017).
55. Phillips, J. C. et al. Scalable molecular dynamics on CPU and GPU architectures with NAMD. *J. Chem. Phys.* **153**, 044130 (2020).
56. Huang, J. et al. CHARMM36m: an improved force field for folded and intrinsically disordered proteins. *Nat. Methods* **14**, 71–73 (2017).
57. R Core Team. R: a language and environment for statistical computing. R Foundation for Statistical Computing. https://www.R-project.org (2021).
58. Humphrey, W., Dalke, A. & Schulten, K. VMD: visual molecular dynamics. *J. Mol. Graph.* **14**, 33–38 (1996).

Acknowledgements

This work was supported by the National Institutes of Health Institute of General Medicine grant R01GM144836. Computational resources have been provided by the Texas Advanced Computing Center (TACC) and Anton 2. Anton 2 computer time was provided by the Pittsburgh Supercomputing Center (PSC) through Grant R01GM116961 from the National Institutes of Health. The Anton 2 machine at PSC was generously made available by D.E. Shaw Research.

Author contributions

A.A.G. conceived and designed the project; M.K.A. performed the simulations; M.K.A. and A.A.G. analyzed the data and wrote the paper.

Competing interests

The authors declare no competing interests.

Additional information

Supplementary information The online version contains supplementary material available at https://doi.org/10.1038/s42003-023-05487-6.

Correspondence and requests for materials should be addressed to Alemayehu A. Gorfe.

Peer review information *Communications Biology* thanks Phillip Stansfeld and the other, anonymous, reviewer(s) for their contribution to the peer review of this work. Primary Handling Editors: Yun Luo, Gene Chong, and Tobias Goris.

Reprints and permission information is available at http://www.nature.com/reprints

Publisher's note Springer Nature remains neutral with regard to jurisdictional claims in published maps and institutional affiliations.

Open Access This article is licensed under a Creative Commons Attribution 4.0 International License, which permits use, sharing, adaptation, distribution and reproduction in any medium or format, as long as you give appropriate credit to the original author(s) and the source, provide a link to the Creative Commons licence, and indicate if changes were made. The images or other third party material in this article are included in the article's Creative Commons licence, unless indicated otherwise in a credit line to the material. If material is not included in the article's Creative Commons licence and your intended use is not permitted by statutory regulation or exceeds the permitted use, you will need to obtain permission directly from the copyright holder. To view a copy of this licence, visit http://creativecommons.org/licenses/by/4.0/.

© The Author(s) 2023